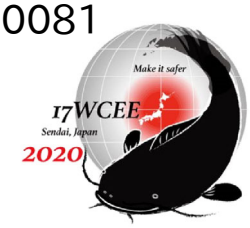

17th World Conference on Earthquake Engineering, 17WCEE
Sendai, Japan - September 13th to 18th 2020

EXPERIMENTAL STUDY ON BEHAVIOR OF COMPOSITE BEAM IN PASSIVELY CONTROLLED BUILDING： FINDING FROM REDUCED－SCALE SUBASSEMBLIES

Y. Matsuda [1], K. Takeshita[2], C. Abe[3], T. Maegawa[4], H. Kinugasa[5]

[1] *Assistant Professor, Tokyo Univ. of Science, Japan, matsuda_y@rs.tus.ac.jp*

[2] *Graduate Student, Tokyo Univ. of Science, Japan, 7119553@ed.tus.ac.jp*

[3] *Graduate Student, Tokyo Univ. of Science, Japan, chakichaki2173@outlook.jp*

[4] *Technical Division, Kumagai Gumi Co., Ltd., Japan, tmaegawa@ku.kumagaigumi.co.jp*

[5] *Professor, Tokyo Univ. of Science, Japan, kinu@rs.noda.tus.ac.jp*

Abstract

Construction of passively controlled buildings by incorporating dampers that enable damage control and response reduction is widespread, and this approach is especially applied in steel buildings to which dampers can be attached firmly. The frames of passively controlled buildings are typically composed of steel beams, columns, gusset plates, and concrete slabs. These members are designed to stay somewhat elastic, but they have sufficient stiffness and strength so that the damper can function sufficiently. When an earthquake damages these members to an extent beyond the design assumptions, each member moves with its own nonlinear behavior and the overall frame behavior is governed by interactions of the nonlinear behavior. Therefore, it is highly necessary to accurately investigate the elastoplastic behavior of a passively controlled building.

However, many studies focusing on the frame of a passively controlled building and the elastoplastic behavior of its components have ignored the concrete slab, and only a few studies have included the slab. As far as the authors know, the effects of the nonlinear behavior of concrete slabs on the frame behavior in a passively controlled building have not been studied.

In this paper, loading tests of a subassembly with a steel damper were conducted to clarify the effect of the concrete slab on the frame of a passively controlled building. The tested subassemblies were half-scale frames of a full-scale five-story steel building with a damper, and they cover one span and one story. One was constructed with a concrete slab and the other did not have a concrete slab.

Keywords: Passively controlled building, steel structure, concrete slab, damper, gusset plate, elastoplastic

1. Introduction

Buildings passively controlled by dampers can minimize damage and reduce the shaking response during earthquakes, and such dampers are especially applicable to steel structures, where the dampers can be firmly attached. Frames with dampers are typically composed of steel beams, columns, gusset plates, and concrete slabs. If the stiffness and strength of these components are optimal, the damper can function sufficiently. In addition, a passively controlled building is designed with the goal of staying elastic, but when it is damaged by very strong seismic motion, non-linear behaviors unique to each component occur, and the overall behavior is governed by their interaction.

Many studies focusing on frames with dampers and the elastoplastic behavior of its components have ignored the concrete slabs [1]. As far as the authors know, no study has been conducted focusing on the influence of the nonlinear behavior of the slab on the interaction of each component and the behavior of the frame with a damper. For this reason, it was necessary to conduct a study that encompassed the effects of the concrete slab.

In this study, to clarify the influence of the concrete slab on other components and the frame with a damper, we conducted a loading test on reduced-scale subassemblies. This paper describes and discusses the results.

2. Test Scheme

2.1 Detail of Subassemblies

As shown in Figure 1, this test reproduces the effect of a story drift angle acting on the building. Then, the bending moment due to story drift and the vertical and horizontal forces due to the damper act on the frame. Two subassemblies were created, one with concrete slabs and another without concrete slabs.

Figure 2 shows the subassembly with concrete slabs. Both subassemblies are one-story, one-span partial frames that are half the size of the five-story test specimens used for E-defense [1]. Each subassembly consists of steel beams, columns, gusset plates, and four types of stiffener. The steel beams are built-up sections of typical BH-200×100×6×9, the columns are square box sections □-175×175×9, and the gusset plates are 9 mm thick. The beams, vertical and horizontal sides, and column stiffeners are 6 mm thick and welded to steel beams, gusset plates, and columns, respectively. When the

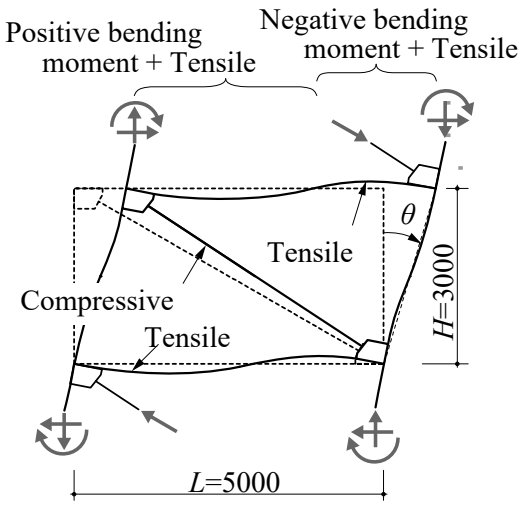

Figure 1 Example of deformed shape and acting force of frame with damper

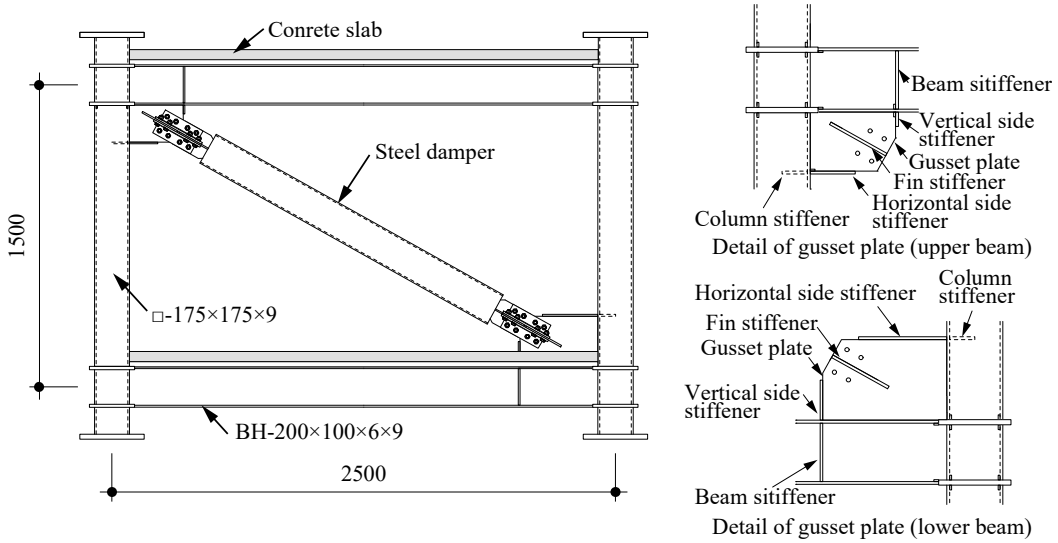

Figure 2 Subassembly with concrete slab

damper is attached, the base line intersects the column centroid at a position 51 mm eccentric to the inside of the frame in the upper left and right panels.

Figure 3 shows the concrete slab shape and locations of strain gages. The concrete slab consists of a deck plate with a height of 25 mm and thickness of 0.8 mm, 50 mm of concrete, and D10 deformed reinforcing bars. The concrete was blended as F_c = 21 N/mm^2. The concrete slab width is 1.3 times the effective width (800 mm) determined by the design recommendations for composite construction [2]. Headed studs (shaft diameter 10 mm, nominal length 50 mm) were placed singly at 75-mm intervals directly on the steel beam web. The composite beam of the subassemblies was designed as a fully composite beam. Tables 1 and 2 show the material test results for the steel and concrete, respectively, used in the subassemblies.

Figure 4 shows details of the steel damper. The damper section attached to the gusset plates is a 9-mm cruciform, the plasticized section is a 9-mm flat bar (SN400B), and its buckling is restrained by mortar and a circular steel tube.

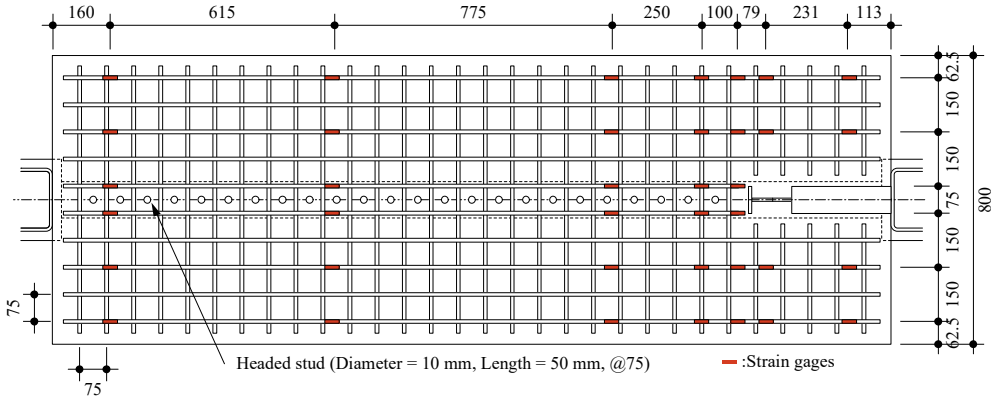

Figure 3 Plan view of concrete slab and location of strain gages

Table 1 Mechanical properties of steel

Member			Yield strength (N/mm^2)	Tensile strength (N/mm^2)	Yield ratio (%)	Rupture elongation (%)
Steel beam (SN490B)	flange	9mm	387	534	72	34
	web	6mm	406	526	77	33
Column (BCR295)		9mm	386	497	78	35
Gusset plate (SM490A)		9mm	378	526	72	36
Damper core (SN400B)		9mm	315	450	70	29
Steel bar (SD295, D10)			360	496	73	19

Table 2 Mechanical properties of concrete

Young's modulus (N/mm^2)	Compressive strength (N/mm^2)	Tensile strength (N/mm^2)
30	27	7

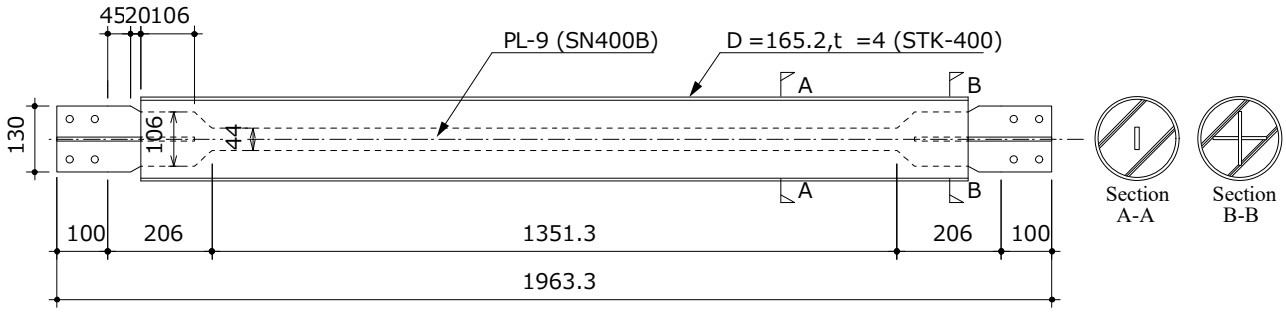

Figure 4 Detailed view of damper

2.2 Loading and Measurement Scheme

Figure 5 shows the test setup. The lower part of the subassembly was fastened to the reaction floor via clevises and loading columns. In the upper part, a 1000-kN jack and a loading beam were horizontally attached to the reaction wall, and these and the subassembly were fastened together via clevises. In addition, the loading beam and the steel frame were tied together with a pantograph to restrain out-of-plane deformation. During loading, the target story drift angle θ was imparted by the 1000-kN jack.

The drift angle θ is obtained from the absolute displacements u_{x1}, u_{x2}, u_{x3}, and u_{x4} of the four panels by the following equation:

$$\theta = \frac{u}{h}, \quad u = \frac{(u_{x1}+u_{x2})-(u_{x3}+u_{x4})}{2}, \qquad (1a, b)$$

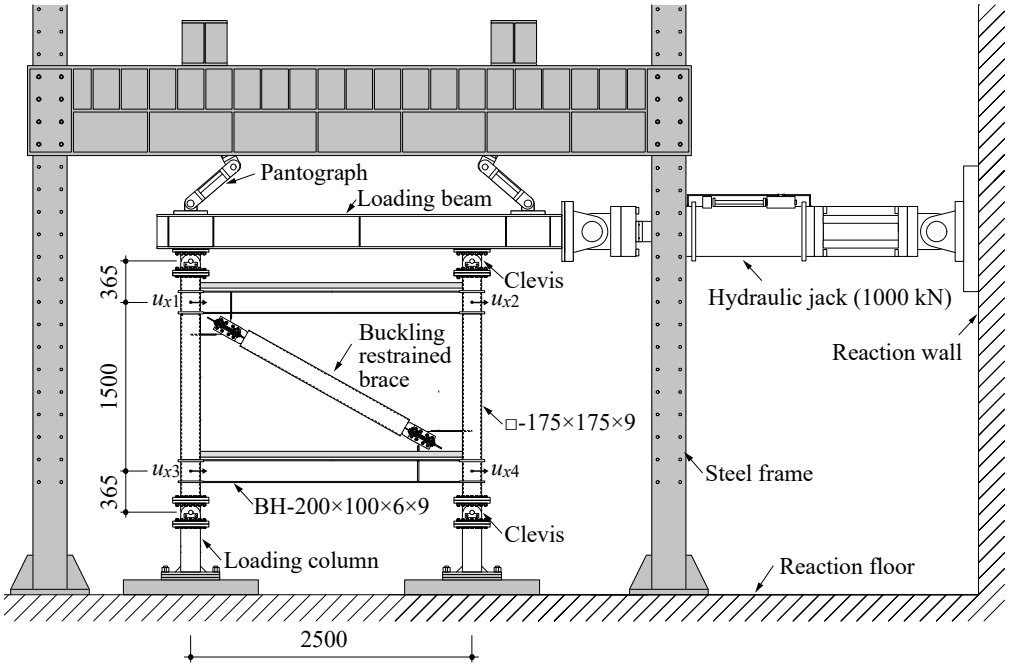

Figure 5 Test setup

where the locations for measuring u_{x1}, u_{x2}, u_{x3}, and u_{x4} are shown in Figure 5.

Figure 6 shows the locations of strain gages. Strain gages were attached to four different types of beam section. Section A is near the column surface on the side without a gusset plate, Section B maintains elasticity until failure occurs, Section C is near the gusset plate on the same side as the gusset plate, and Section D is the section with a gusset plate. The largest damage occurred in Sections A and C. The section identifiers ending with U are on the upper beam, and those ending with L are on the lower beam. Strain gages were attached to two kinds of column sections. Section E maintains elasticity until failure, and Section F is the section with a gusset plate. The section identifiers beginning with L are on the left column, and those beginning with R are on the right column. In the upper and lower gusset plates, rosette strain gages were attached at five and six locations, respectively. In the panel, a rosette strain gage was attached to each location. By measuring the relative deformation of the cruciform section and the circular steel tube, the deformation of the plasticized part of the damper can be obtained.

Figure 7 shows the loading protocol. The magnitude of the story drift angle θ was cyclically increased in both the positive and negative directions. The test applied two cycles each of $\theta = \pm 1/800$, $\pm 1/400$, $\pm 1/200$, $\pm 1/100$, $\pm 1/67$, $\pm 1/50$, and $\pm 1/33$ rad. After completing these 14 cycles (incremental loading), repeated cycles of $\theta = \pm 1/33$ rad were applied until failure (repeated loading).

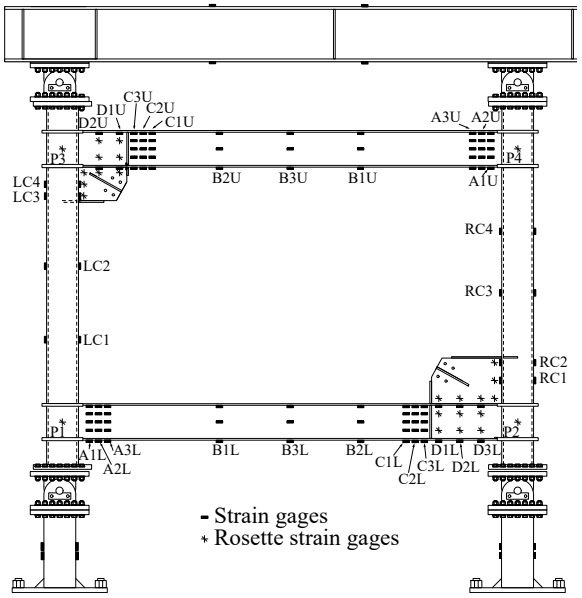

Figure 6 Locations of strain gages in steel portion

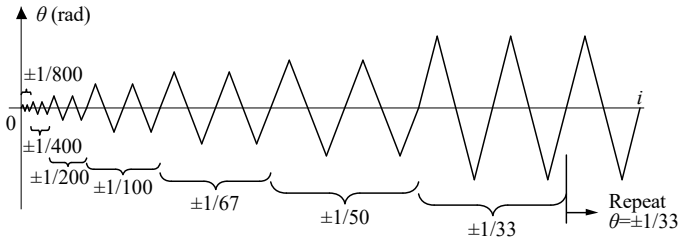

Figure 7 Story drift control protocol

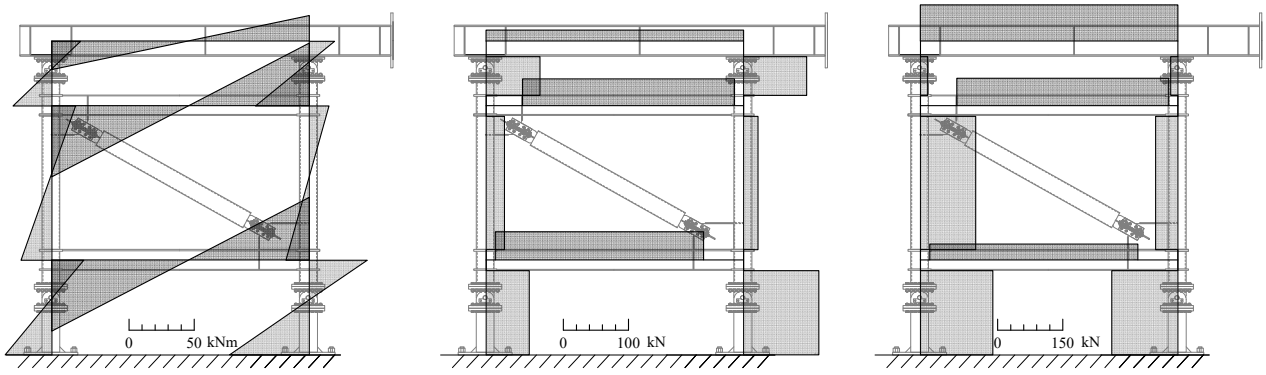

Bending moment Shear force Axial force

Figure 8 Internal force distribution

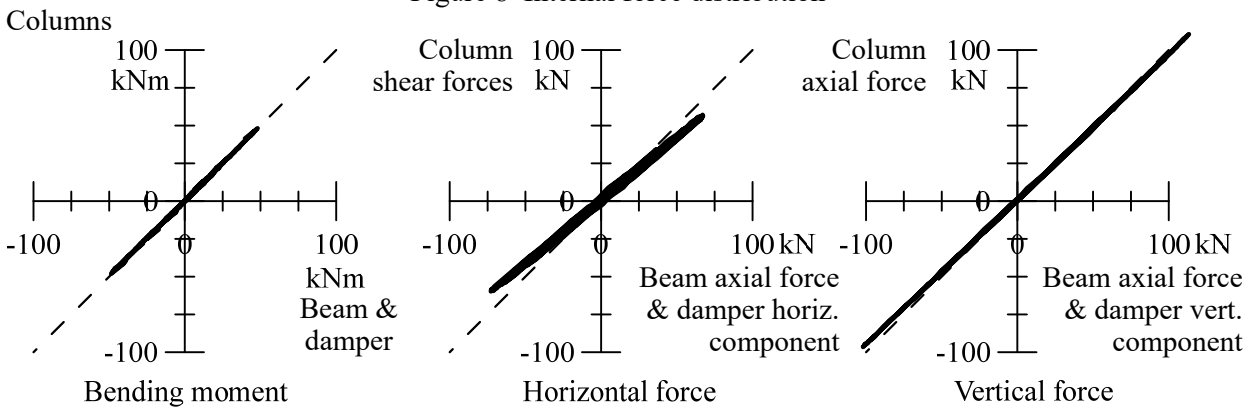

Figure 9 Equilibrium at intersection of the upper left beam and column

3. Results of Incremental Loading Tests

3.1 Equilibrium at the beam and column intersection

Figure 8 shows the internal force distribution of subassembly without a concrete slab at θ = 1/200, and Figure 9 shows equilibrium at the intersection of the upper beam and left column. The bending moment distribution was obtained by linearly interpolating and extending the bending moment obtained from two strain measurement sections for each member, and the shear force distribution was obtained from the gradients of the bending moment distribution. To obtain the moment distribution of the beam, the strains of sections B1U and B3U were used for the upper beam and sections B1L and B3L were used for the lower beam. To obtain the moment distribution of the beam, the strains of sections B1U and B3U were used for the upper beam and sections B1L and B3L were used for the lower beam. The axial force distribution was obtained by an average value obtained from two measurement cross sections. In addition, the eccentric bending of the damper is added to the equilibrium in Figure 8a. Figure 8 confirms that the bending moment, horizontal force, and vertical force are roughly balanced. In the subassembly with a concrete slab, the loading position of the axial force on the composite beam cross section is unknown and the moment cannot be calculated. Thus, the stress distribution in the subassembly with concrete slab was calculated from the equilibrium of the column, jig, and damper at the column and beam intersections.

3.2 Behaviors of the subassemblies and dampers

The relationship between the shear force of the parallel system of frame and damper Q_s, the frame shear force Q_f, and the horizontal component of the damper force Q_d is as follows:

$$Q_s = Q_f + Q_d\,,\quad Q_f = Q_{cL} + Q_{cR} \qquad \text{(2a, b)}$$

where Q_s is the value of the jack load cell and Q_{cL} and Q_{cR} are the shear forces in the left and right columns, respectively, obtained as the gradient of the bending moment distribution. Figure 10 shows the $Q_f - \theta$ relationship up to the second cycle of the maximum drift angle θ = 1/33. When the concrete slab is present, the maximum shear force Q_f increases 1.29 times on the positive loading and 1.21 times on the negative loading, and the initial stiffness ($Q_f - \theta$ slope at θ = 1/200) increases 1.53 times on the positive loading and 1.41 times on the negative loading. The stiffness at the unloading has decreased. This is due to the high stiffness of the damper, which imposes a large horizontal force on the damper and reduces the shearing force on the frame (Eq. 2a) [3]. Figure 11 shows the $Q_d - \theta$ relationship up to the second cycle of the maximum drift angle θ = 1/33. In both the specimens with and without a concrete slab, the damper yielded in the cycle of θ = ±1/400, and the histories after that were almost the same. These results indicate that the presence of the concrete slab has almost no effect on the damper history.

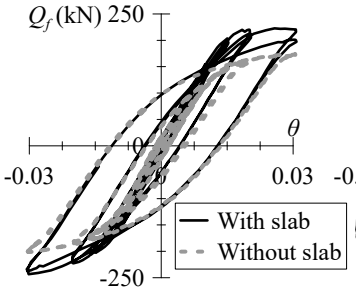

Figure 10 $Q_f - \theta$ (frame action)

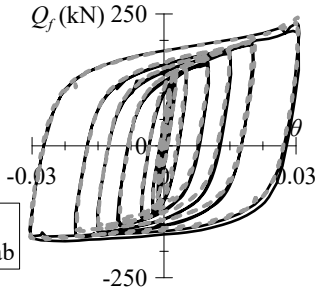

Figure 11 $Q_d - \theta$ (damper action)

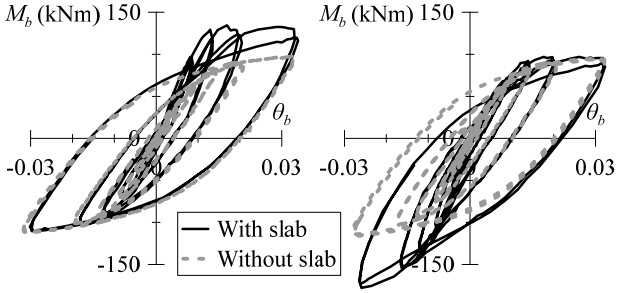

(a) Upper left (b) Lower right

Figure 12 $Q_b - \theta_b$ (beam action)

Figure 12 shows the relationship between beam bending moment M_b and beam deformation angle θ_b at the beam and column intersection. The beam deformation angle was obtained from the curvature of the strain measurement sections. Specifically, it was obtained by integrating the curvature distribution between the center of the member and the column surface to obtain the beam deformation, and then dividing it by half of the beam length [4]. The bending moment and deformation angle are positive for clockwise rotation. At the

positive bending moment, the θ_b of the subassembly with the concrete slab was smaller than that of the subassembly without the concrete slab. This is because θ_b with respect to θ has decreased due to an increase in the stiffness of the beam.

Figure 13 shows the transition of the hysteresis energy of the beam $\Delta W'_b$ and the damper $\Delta W'_d$ for two cycles of each target story drift angle. $\Delta W'_b$ is the sum of the values obtained from the relationship between the beam bending moment and the beam deformation angle at four intersections. $\Delta W'_d$ increased in both subassemblies after the cycle of θ = ±1/400, when the damper yielded, and absorbed four to five times more than $\Delta W'_b$ in the cycle of θ = ±1/100. $\Delta W'_b$ is small for both specimens because the damage to the beam is slight up to the cycle of θ = ±1/100. The reason why the $\Delta W'_b$ of the subassembly with the concrete slab was slightly larger than without the concrete slab is considered to be that slight damage occurred to the concrete slab. After that, $\Delta W'_b$ increased as the plastic region of the beam increased, and it was almost equal to $\Delta W'_d$ in the cycle of θ = ±1/50, and 1.2 to 1.3 times $\Delta W'_d$ in the cycle of θ = ±1/33.

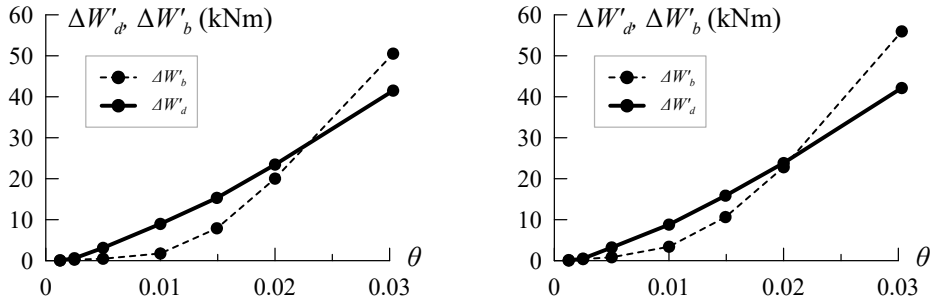

(a) Without concrete slab (b) With concrete slab

Figure 13 Transition of the hysteresis energy of the beam $\Delta W'_b$ and damper $\Delta W'_d$

3.3 Strain behaviors

Figure 14 shows the strain distribution on the concrete slab obtained from the reinforcing bars at θ = ±1/200, when compressive strain occurred in the concrete slab. Except for cross sections C1L and C3L, the strain reached its maximum near the beam web and decreased with distance from the web. The same tendency was observed in sections D1L and D3L, where the studs were not welded, because the gusset plate was attached. In the lower beam, the strain above the beam web in cross sections C1L and C3L near the

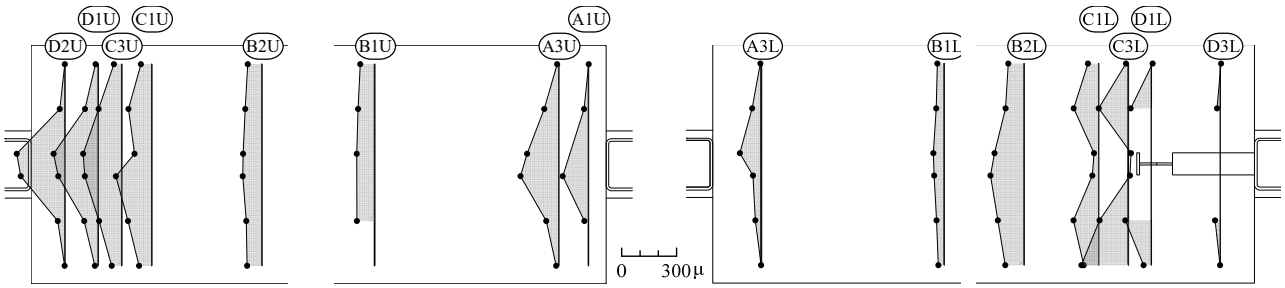

(b) Upper left (θ = +1/200) (b) Upper right (θ = -1/200) (c) Lower left (θ = +1/200) (d) Lower right (θ = -1/200)

Figure 14 Strain distribution on concrete slab at θ = ±1/200

gusset plate (Figure 14d) was close to zero.

Figure 15 shows the behavior of the lower composite beam, which can explain the behavior discussed above. At the beam end where the positive bending acts, the composite beam and the column bear the bending moment of reverse rotation, so that the slab and the column come into contact and the concrete slab is subjected to compressive force. Therefore, in cross sections D1L and D3L, the concrete slab was subjected to compressive strain during negative loading. In contrast, in cross sections C1L and C3L, as shown in

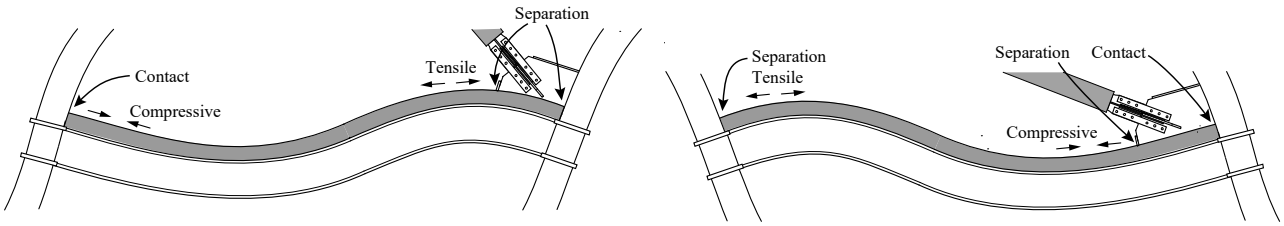

(a) Positive loading case (b) Negative loading case

Figure 15 Behavior of lower composite beam

Figure 15, the composite beam and the vertical side stiffener received the same rotational moment. Therefore, because the concrete slab does not contact the vertical side stiffener, no strain occurred around the vertical side stiffener. Figure 16 shows the effective width distribution in the lower concrete slab. The effective width B_i is defined as the width of a rectangle having the same area as the measured strain distribution and the maximum absolute value of the strain. B_i is expressed by Equation 3 and Figure 17 [5].

$$B_i = \frac{\Sigma\left(\frac{\varepsilon_{i,j}+\varepsilon_{i,j+1}}{2}\right)\times\left(l_j - l_{j+1}\right)}{\varepsilon_{i,max}}, \quad (3)$$

where j is the position of the cross section and $\varepsilon_{i,max}$ is the maximum absolute value of the strain of the target cross section at step i. For cross sections C1L and C3L, where the strain gauges were not attached just above the beam web, B_i was calculated using the strain obtained by extending the inclination of the two measurement points to just above the beam web. The length of the effective width tends to be short near the beam end, and it is about half the value indicated by Japanese design recommendations (1200 mm [2]) near the beam center. Further, the effective width is shorter in cross sections C1L and C3L, where no strain occurred near the vertical side stiffeners, in contrast with the other cross sections. It is confirmed that B_i in the negative loading case is smaller than that in the positive loading case. This is considered to be due to the

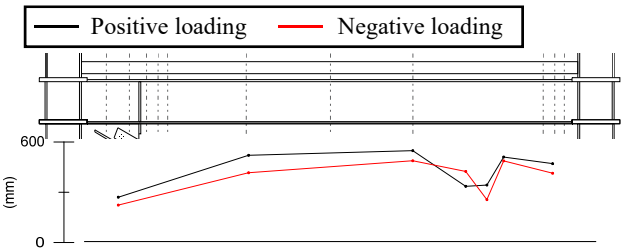

Figure 16 Effective width B_i distribution

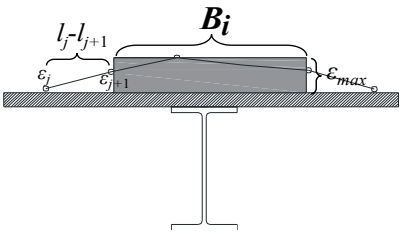

Figure 17 Calculation method of effective width B_i

influence of the bearing between the slab and the vertical side stiffener described above.

Figure 18 shows the bending moment distribution of the upper beam at θ = ±1/200, and Figure 19 shows the strain distributions at the upper and lower beam sections at θ = ±1/200. The strain value of the concrete slab was obtained by the average of the two strains just above the beam web. Comparison of the two subassemblies confirms that the strain in the lower flanges is the same even when subjected to a positive bending moment, except for cross section B1U near the inflection point (Figure 18). This is because when the concrete slab is attached, the neutral axis position rises, but the strain is less likely to occur due to the increase in moment inertia [6]. When the composite beam was subjected to negative bending, the two strain distributions were almost the same, indicating that the concrete slab is not effective. The strain of the slab was smaller than the distortion of the upper flange. This is because the deformation of the stud causes a slip between the concrete slab and the steel beam [7], and it is difficult for stress and strain to be transmitted to the slab.

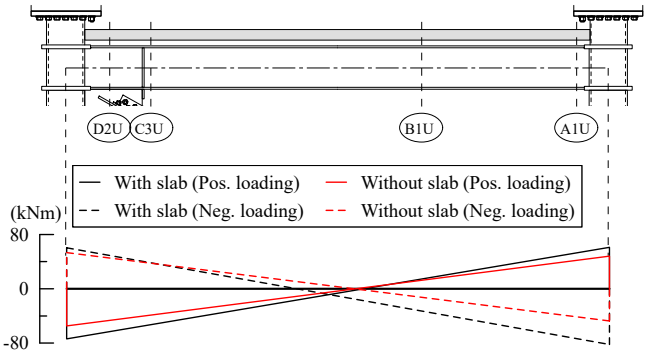

Figure 18 Bending moment distribution in upper beam at $\theta = \pm 1/200$

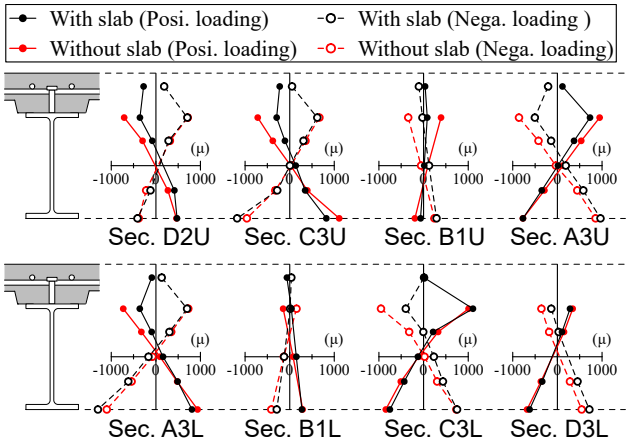

Figure 19 Strain distribution in composite beam at $\theta = \pm 1/200$

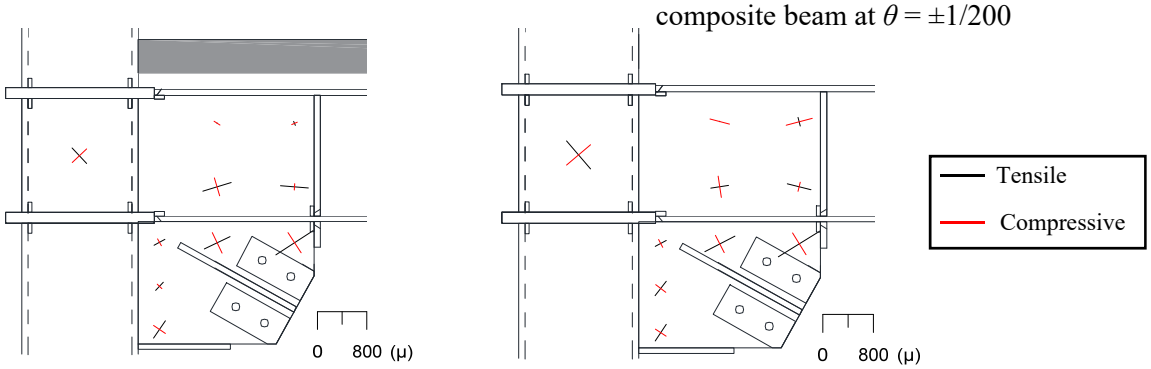

(b) With concrete slab (a) Without concrete slab

Figure 20 Principal strain distributions at $\theta = \pm 1/200$

Figure 20 shows the magnitude and direction of the principal strain around the gusset plate in the first cycle of $\theta = +1/200$. The principal strain of the gusset plate does not differ with the presence or absence of the concrete slab. The beam moment on the cross section with a gusset plate of the subassembly with the concrete slab was about 1.3 times larger than that of the subassembly without the concrete slab (Figure 18). However, such a result was obtained because strain was less likely to occur due to an increase in cross-sectional performance owing to the presence of the slab.

4. Results of Constant Cycle Loading Tests

Figure 21 shows the relationship between Q_f and the number of cycles during constant cycle loading. The circled numbers in Figure 21 indicate the order in which the members were damaged. Figure 22 shows the condition of each damaged member. Hereafter, only the subassembly with the concrete slab is described. It was confirmed that Q_f gradually decreased during both positive and negative loading. It was visually confirmed that local buckling occurred in the beam web from the first cycle, and it is considered that this progressed and Q_f decreased. At the 9th cycle, the core material of the damper broke (①), and the Q_f increased accordingly (Eq. 1a) to reach the maximum yield strength. Immediately after that, a crack was formed in the lower flange on the left end of the lower beam. This crack became larger as the loading progressed, and the lower flange fractured (②) at the 13th cycle. After that, the crack progressed to the web and Q_f decreased gradually. Finally, at the 49th cycle, the lower flange near the gusset end of the upper beam broke (③), and then at the 55th cycle, the Q_f reached half of the maximum value. With respect to the subassembly without the concrete slab, each fracture property was confirmed with a number of cycles similar to that of the specimen with the slab (① = 12th, ② = 19th, ③ = 58th cycle).

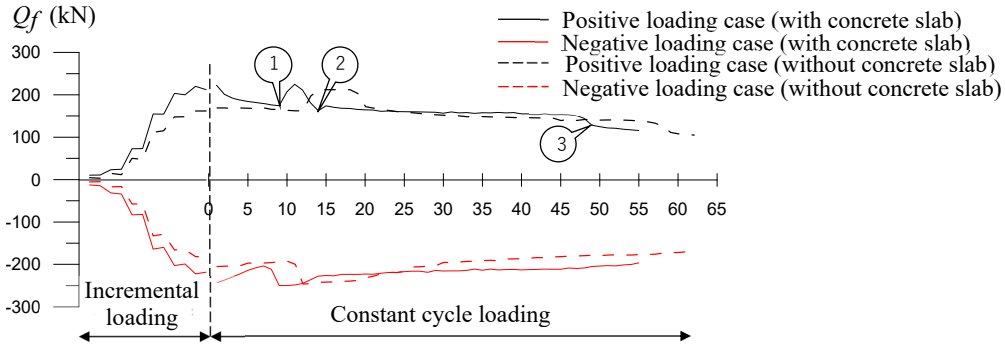

Figure 21 Relationship between Q_f and number of cycles

(a) ① Broken core material of the damper

(b) ② Fracture of lower flange (lower beam, left side)

(c) ③ Fracture of lower flange (upper beam, left side)

(d) Locations of fractures

Figure 22 Condition of each fracture

5. Conclusions

The following conclusions were obtained from the tests of the two subassemblies:

1. It was confirmed that the concrete slab increased the stiffness and strength of the beam in the subassembly. In contrast, the damper behaviors were the same with and without the concrete slab.
2. The energy absorption of the beam increased after the cycle of $\theta = \pm 1/100$. Compared to the absorbed hysteretic energy of the damper, it was almost the same during the cycle of $\theta = \pm 1/50$ and 1.2 to 1.3 times higher in the cycle of $\theta = \pm 1/33$.
3. Around the lower gusset plate, the concrete slab and the vertical side stiffener are not in contact with each other, so that bearing pressure from the vertical side stiffener cannot be expected. Therefore, in this vicinity, the strain of the concrete slab directly on the beam web was almost zero, and the effective width was calculated to be short.
4. The subassembly with the concrete slab produced a larger beam bending moment than the subassembly without the concrete slab, but the principal strains on the gusset plates and bottom flange of steel beams were the same as in the subassembly without the concrete slab. This is because strain is less likely to occur due to an increase in cross-sectional performance owing to the presence of the concrete slab. For the same reason, strain in the gusset plates of the subassembly with the concrete slab had the same value as in the subassembly without the concrete slab.

5. In both subassemblies, the core of the damper broke first, then the lower flange on the left end of the lower beam cracked, and finally the lower flange on the left end of the upper beam cracked, leading to failure.

References

[1] Kasai, K., Baba, Y., Nishizawa, K., Hikino, T., Ito, H., Ooki, Y., Motoyui (2012): Test results for building with steel dampers, 3D shake table tests on full scale 5-story steel building with dampers Part2. *J. Struct. Constr. Eng.,* No.673, pp. 499-508

[2] Architecture Institute of Japan (2010). Design Recommendations for Composite Constructions.

[3] Kasai, K.,Watanabe, Y., Minato, N. (2005): Study on dynamic behavior of a passive system with visco-plastic Damper. *J. Struct. Constr. Eng.,* No.588, pp. 87-94

[4] Kasai, K.,Matsuda, Y., Motoyui, S., Kishiki S. (2015): Fundamental Study using New Test Loading Scheme for Steel Frame Subassembly with Damper Connection Details. *J. Struct. Constr. Eng.,* No.708, pp. 309-319

[5] Yamanobe, K.,Yabe, Y., Wada, A. (1996): Lateral loading test on steel frames with 3-spanned continuous composite beams. *J. Struct. Constr. Eng.,* No.487, pp. 121-129

[6] Matsuda, Y.,Kasai, K., Sakai, S. , Motoyui, S. (2016): Basic Study on Behavior of Composite Beam Subjected to Double Curvature Bending. *J. Struct. Constr. Eng.,* No.722, pp. 791-801

[7] M.N. Newmark et.al.(1951):Test and analysis of composite beams with incomplete interaction , Proc. Of the Society of Experimental Analysis, Vol.9,no.1

